Hover Handling Qualities of Fixed-Pitch, Variable-RPM Quadcopters of Increasing Size





Ariel Walter* *Ph.D. Student*
Michael McKay *Ph.D. Graduate*
Robert Niemiec *Research Scientist*
Farhan Gandhi *Redfern Professor, Director*
Center for Mobility with Vertical Lift (MOVE), Rensselaer Polytechnic Institute, Troy, NY
Christina Ivler *Assistant Professor*
University of Portland
Portland, OR

Fixed-pitch, variable-RPM quadcopters of increasing size are simulated in hover. Three aircraft sizes are considered, with rotor diameters of 4, 6, and 8 ft (1.2, 1.8, and 2.4 m) and gross weights of 300, 680, and 1200 lb (136, 308, and 544 kg) respectively. Control design is performed for each aircraft using CONDUIT®, first using standard ADS-33E-PRF handling qualities specifications. Froude scaling is then applied to the specifications in order to design more comparable, aggressive controllers for the two smaller aircraft. Piloted commands and gust inputs are simulated in the time domain in order to estimate the necessary motor current margins needed for adequate maneuverability local to hover. Of the maneuvers considered, a yaw rate step requires the highest current margin for the smallest aircraft, while the longitudinal velocity step requires the highest current margin for the others, regardless of the Froude scaling of the handling qualities metrics. Using the maximum current values from these simulations, the motor weight fraction is 8.3–10.6% for the 300-lb vehicle, 11.6–13.0% for the 680-lb vehicle, and 15.8% for the 1200 lb. Motor weight requirements can be reduced on the larger two aircraft by flying with the pitch and roll axes exclusively in the attitude command, attitude hold mode, rather than translational rate command. In this case, step commands in yaw rate are limiting for the 680-lb vehicle (10.7–11.8% motor weight fraction) and heave commands are limiting for the 1200-lb vehicle (13.6% motor weight fraction). Estimated motor weight requirements are also reduced by decreasing the rotor inertia and introducing additional filtering into the aircraft commands.

Nomenclature

I_{rotor}	rotor inertia
i	motor current
K	open-loop-onset-point constant
K_e	motor back-EMF constant
K_t	motor torque constant
L	motor inductance
M_{motor}	motor mass
N_{rotors}	number of rotors
R	rotor radius
R_m	motor resistance
r	yaw rate
Q	motor torque
Q_A	rotor aerodynamic torque
U	control inputs
u	longitudinal velocity
V	motor voltage
v	lateral velocity
w	heave rate
W_{motor}	motor
X	dynamic states
θ	pitch attitude
ϕ	roll attitude
ψ	heading
Ψ_k	rotor k azimuthal location
Ω	rotor speed
$\dot{\Omega}$	rotor acceleration
ACAH	attitude command, attitude hold
eVTOL	electric vertical takeoff and landing
FB	feed-back
FF	feed-forward
HQ	handling qualities
OLOP	open-loop-onset-point
RCDH	rate command, direction hold
RMAC	Rensselaer Multicopter Analysis Code
RMS	root mean square
RPM	rotations per minute
TRC	translational rate command
UAM	urban air mobility

Introduction

With the push for the development of urban air mobility (UAM), a large variety of electric vertical takeoff and landing (eVTOL) aircraft designs have been proposed, but the field still faces many challenges

*Corresponding author: Email: waltea@rpi.edu.
Presented at VFS 76th Annual Forum & Technology Display, Virtual, October 5–8, 2020. Manuscript received August 2021; accepted April 2022.

Table 1. Rotor geometry

Parameter	Value
Rotor solidity	0.09
Taper ratio	2.5
Root pitch	21.5°
Tip pitch	11.1°

before large eVTOL aircraft become commonplace (Ref. 1). One of these challenges is the scalability of fixed-pitch, variable-RPM multirotor systems, which are common on eVTOL aircraft.

Though fixed-pitch, variable-RPM rotors are commonly used on small-scale, unmanned multirotor aircraft, their effectiveness for control of larger, UAM-scale vehicles is still under examination. Handling qualities (HQ) requirements specific to these aircraft have not yet been officially established, but the current Aeronautical Design Standard, ADS-33E-PRF (Ref. 2), which defines HQ metrics for manned military helicopters, can be applied to UAM aircraft. It has previously been shown (Refs. 3–5) that large eVTOL aircraft which rely on changing the rotational speed of large rotors for control may not be able to meet these HQ requirements without significantly larger, higher torque motors (and thus, power-train weight) than would otherwise be required on such an aircraft.

The purpose of this study is to examine the effects of increasing aircraft size on the motor requirements for a variable-RPM quadcopter to meet HQ specifications. A single passenger-sized (1200 lb) quadcopter will be considered as a baseline and compared to two smaller aircraft with equivalent disk loading. The aircraft will first be held to standard HQ requirements, then the requirements for smaller aircraft will then be tightened via Froude scaling, requiring the smaller aircraft to essentially be more maneuverable. The metrics defined in the ADS-33E-PRF have previously been scaled and applied to smaller, unmanned aircraft, such as Ref. 6 where Froude scaling is applied to obtain scaled requirements for the IRIS+ quadcopter by scaling to the maximum velocity of the UH-60 Black Hawk. Similarly, length-based Froude scaling was used in Ref. 3 to examine the scaling of HQ specifications on quadcopters of different sizes. This previous study found that, with a motor power saturation limit included, larger fixed-pitch quadcopters were unable to meet disturbance rejection bandwidth requirements with the assumed motor parameters, especially in yaw. The present study instead relaxes the installed power (motor size) assumption and examines similar quadrotor aircraft of different gross weights in order to estimate the motor size required for the aircraft to perform adequately with respect to published HQ requirements.

Modeling and Analysis Tools

Platform

The aircraft considered in this study are cross-type quadcopters with a tip-to-tip clearance of 10% of the rotor radius. Each rotor is directly driven by a dedicated electric motor. A simple representation of the quadcopter configuration, including rotor/motor numbering and spin direction, is shown in Fig. 1. Froude-scaled aircraft with 4, 6, and 8 ft (1.2, 1.8, and 2.4 m) rotor diameters are simulated. The disk loading is held constant at 6 lb/ft^2 (287 N/m^2) for all vehicle sizes considered, resulting in aircraft gross weights of 300, 680, and 1200 lb (136, 308, and 544 kg).

The rotor geometry used is summarized in Table 1. The airfoil sections are assumed to be a NACA4412 at the root of the blade and a Clark Y at the tip, with linear interpolation in between (as in Ref. 7). The rotor parameters are scaled based on their diameter for use on the large quadcopters being considered, holding pitch distribution, solidity, and taper ratio constant across the configurations.

The rotational inertia of the fuselage is based on a scaled version of the single-passenger NASA Concept quadcopter presented in Ref. 1. These scaled inertias are given in Table 2, along with other aircraft parameters including the hover current and power input to each motor.

As shown in Fig. 2, rotor inertia is approximated based on data from existing rotors (Refs. 8, 9). A curve is fit to the data assuming that rotor

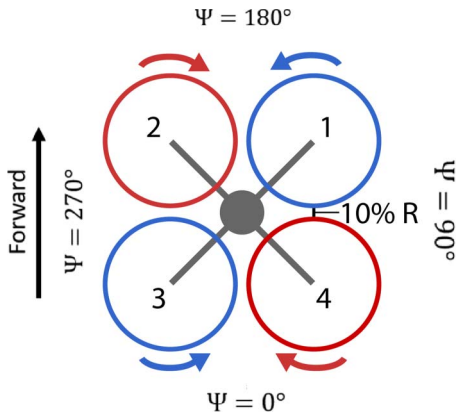

Fig. 1. Quadcopter configuration with rotor numbering.

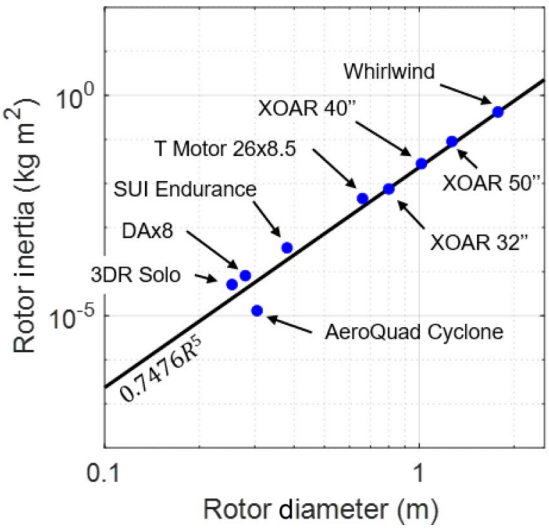

Fig. 2. Approximation of rotor inertia.

Table 2. Aircraft parameters

Parameter Rotor Diameter (m)	1.2	1.8	2.4
Gross weight (kg)	136	308	544
Rotor inertia (kg m^2)	0.063	0.480	2.014
Hover current (A)	75	112	150
Hover power (kW)	21	48	85
I_{xx} (kg m^2)	43	173	467
I_{yy} (kg m^2)	51	204	549
I_{zz} (kg m^2)	84	334	905
K_e and K_t	0.30	0.66	1.18

inertia is proportional to radius to the fifth power, yielding the estimation $I_{\text{rotor}} = 0.7476R^5$ (R^2 of 0.99), where R is the rotor radius in m and I_{rotor} is the inertia in kg m^2.

Simulation models

Linearized dynamic simulation models are generated using the Rensselaer Multicopter Analysis Code (RMAC; Ref. 10). This code calculates the forces and moments on the multicopter using blade element theory coupled with a 3×4 Peter–He finite state dynamic wake model (Ref. 11). The dynamic states include the 12 rigid-body states (position, attitude, linear velocity, and angular rate), 10 inflow states per rotor (40 total), and the four-rotor speeds for a total of 56 states. The inputs to the system are a voltage signal to each of the four motors. Since the inflow states are generally very high frequency (on the order of the rotor speed, Ref. 12), they can be reduced out of the linear model via static condensation (assuming instantaneous settling of the inflow states), yielding a reduced-order model with the state and control vectors given by Eqs. (1) and (2), respectively.

$$X = [x \;\; y \;\; z \;\; \phi \;\; \theta \;\; \psi \;\; u \;\; v \;\; w \;\; p \;\; q \;\; r \;\; \Omega_1 \;\; \Omega_2 \;\; \Omega_3 \;\; \Omega_4]^T \quad (1)$$

$$U = [V_1 \;\; V_2 \;\; V_3 \;\; V_4]^T \quad (2)$$

Motor–rotor dynamics are modeled using DC motor equations, as in Ref. 4. The angular acceleration of each motor–rotor system is represented by Eq. (3), where $K_t i$ represents the input motor torque, Q_A is the aerodynamic torque, and viscous losses are neglected. Motor current is represented by Eq. (4), where L is the motor inductance, V is the input voltage, K_e is the back-EMF constant, and $R_m\ i$ is the Ohmic voltage drop across the motor.

$$I_{\text{rotor}}\dot{\Omega} = K_t i - Q_A \quad (3)$$

$$L\frac{di}{dt} = V - K_e\Omega - R_m i \quad (4)$$

Since L is negligible (Ref. 4), it is assumed that the electrical dynamics evolve instantaneously. Equation (4) can then be solved for i and substituted into Eq. (3) to get Eq. (5), where $K_e = K_t$ for SI units. This equation is implemented as the governing equation relating rotor speed to the voltage input to the motor. The motor parameters K_t and R_m are obtained using the methods of Ref. 4 and listed in Table 2.

$$I_{\text{rotor}}\dot{\Omega} = \frac{K_t}{R_m}V - \frac{K_t^2}{R_m}\Omega - Q_A \quad (5)$$

Control mixing is achieved by the multirotor coordinate transform (Eq. (6), Ref. 13), where Ψ_k represents the azimuthal location of rotor hub k on the aircraft (Fig. 1, Eq. (7)). V_0 represents mean voltage, used to control heave. V_{1s} and V_{1c} represent lateral and longitudinal variation in voltage input and thus control roll and pitch. Finally, V_d alternates positive and negative input, producing a yaw moment on the aircraft. Using the multirotor coordinate transform decouples the dynamics of the quadcopter, reducing it to a set of single-input, single-output systems, one each for the longitudinal, lateral, directional, and vertical axes.

$$\begin{bmatrix} V_1 \\ V_2 \\ V_3 \\ V_4 \end{bmatrix} = \begin{bmatrix} 1 & \sin(\Psi_1) & \cos(\Psi_1) & 1 \\ 1 & \sin(\Psi_2) & \cos(\Psi_2) & -1 \\ 1 & \sin(\Psi_3) & \cos(\Psi_3) & 1 \\ 1 & \sin(\Psi_4) & \cos(\Psi_4) & -1 \end{bmatrix} \begin{bmatrix} V_0 \\ V_{1s} \\ V_{1c} \\ V_d \end{bmatrix} \quad (6)$$

$$\Psi_k = (90k + 45)^\circ \quad \text{for } k = 1, 2, 3, 4 \quad (7)$$

Table 3. CONDUIT® inner loop constraints

Specification
Hard constraints
Eigenvalues
Stability margins
Nichols margin
Soft constraints
Bandwidth
Phase delay
Crossover frequency
Disturbance rejection bandwidth
Damping ratio
Model following
OLOP (pilot and disturbance)
Summed objectives
Actuator RMS (pilot and disturbance)
Minimize crossover frequency

For the sake of control design and simulation, the nonlinear model is linearized about a hover trim point. The linear model is validated against the nonlinear model with closed-loop simulations. In hover, the transient response of the linear model is nearly identical to the nonlinear model. As an example, the closed-loop heave response to a −5 m/s step (climb) is plotted in Fig. 3 for both the linear and nonlinear models, along with the change in current input to a single motor during this step.

Control optimization

A standard set of HQ requirements are considered as constraints during control optimization (as recommended in Ref. 14). ADS-33E-PRF (Ref. 2) provides a series of HQ specifications for manned helicopters, such as required piloted bandwidth and minimum damping ratios. Additionally, disturbance rejection requirements (Ref. 15), and open-loop onset point (OLOP) specifications are included in the analysis (Ref. 16). To meet these requirements, a two degree-of-freedom attitude-command-attitude-hold/rate-command-direction-hold (ACAH/RCDH) explicit-model-following control architecture (Fig. 4) is implemented as the inner control loop. Similarly, an outer loop that controls aircraft velocities is wrapped around the inner loop. Within the inner loop, the commanded rotor speeds are filtered through a first-order command model that governs how quickly the rotors are required to change their speed. An inversion of the motor dynamics is used to determine the voltage input signals from the filtered rotor speeds. The differential voltage command bypasses this because the directional response of the aircraft is directly affected by the changes in motor torque, whereas the heave, longitudinal, and lateral responses rely on changes in rotor speeds. The inner loop is designed first, with the feedback gains and command model parameters optimized using CONDUIT® (Ref. 14). The objective of the optimization is to minimize actuator effort while meeting the specifications listed in Table 3. Descriptions of these specifications can be found in Ref. 14.

After tuning the inner loop, the nested loop optimization approach of Ref. 14 is taken. With the inner loop gains frozen, the inner loop specifications are disabled, and the outer loop specifications in Table 4 are used to optimize the gains of a translational-rate-command (TRC) controller. In addition to the standard constraints, the rise time of the translational velocity step responses is constrained to be between 2.5 and 5 s (specified by Ref. 2).

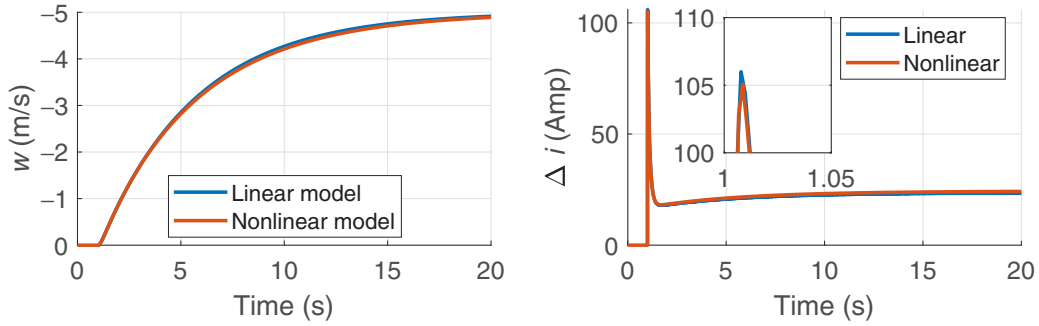

Fig. 3. Comparison of linear and nonlinear models.

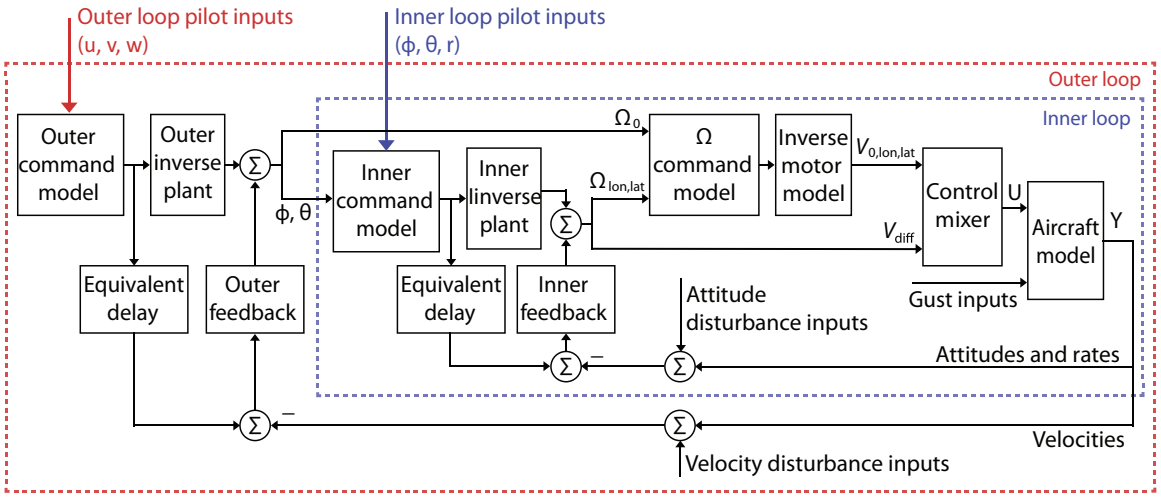

Fig. 4. Controller architecture.

Table 4. CONDUIT® outer loop constraints

Specification
Hard constraints
Eigenvalues
Stability margins
Nichols margin
Soft constraints
Bandwidth
Phase delay
Crossover frequency
Disturbance rejection bandwidth
Damping ratio
Heave mode pole frequency
Heave time delay
Model following
OLOP (pilot and disturbance)
Summed Objectives
Actuator RMS (pilot and disturbance)
Minimize crossover frequency

Table 5. Froude scaling of different dimensions

Dimension	Unit	Scaling
Length	m	F^2
Time	s	F
Attitude	rad	–
Frequency	rad/s	$1/F$
Velocity	m/s	F

An approximate equivalent delay is included within the feedback paths of both the inner and outer loops. In the inner loop, this delay accounts for the lag that is caused by the motor dynamics. In the outer loop, the delay accounts for both the motor dynamics and inner loop dynamics. These delays are included in order to improve the model following at high frequency, which is a nondimensional evaluation of how well the aircraft is able to follow the command model (as defined in Ref. 17). A model following a cost of less than 50 indicates that the command and vehicle response are effectively indistinguishable.

Scaling of specifications

Two types of comparisons are made between the three quadcopters considered in this study. In the first set of comparisons, all three multicopters are held to the same standard, as defined by ADS-33E-PRF for target tracking and acquisition in hover/low speed. The second set of comparisons utilize Froude scaling (Ref. 18) to adjust the HQ requirements based on the presumption that a smaller vehicle is capable of greater agility. The Froude-scaling parameter is given by Eq. (8), where hub-to-hub distance refers to the distance between diametrically opposed rotors.

$$F = \sqrt{\frac{\text{Hub-to-hub distance}}{\text{Reference hub-to-hub distance}}} \tag{8}$$

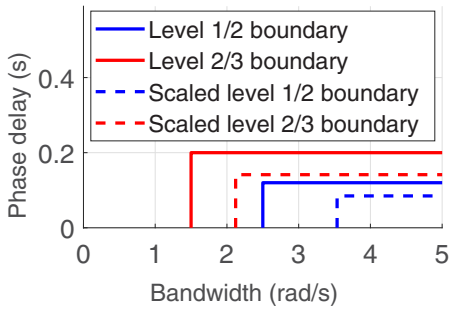

Fig. 5. Scaling of roll bandwidth specification for quadcopter with 1.2 m diameter rotors.

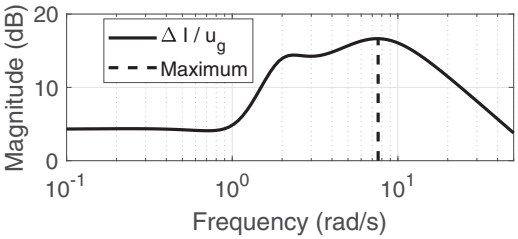

Fig. 6. Magnitude frequency response from gust to motor current.

The HQ of the smaller aircraft is to be scaled with respect to the single passenger scale aircraft. Thus, the reference hub-to-hub distance is that of the 1200-lb quadcopter (3.62 m). This means the largest of the quadcopters is held to the ADS-33E-PRF because it is manned-sized, while the specifications are scaled based on their dimensions (Table 5) for the two smaller vehicles. The roll bandwidth specification within CONDUIT® is shown as an example in Fig. 5. Compared to the unscaled specification, the Froude-scaled version requires 41% higher bandwidth (rad/s) and 41% smaller phase delay (s) to satisfy Level 1.

Evaluation Methods

Aircraft performance is evaluated by simulating step and gust responses in the time domain and examining the current input to the motors during the simulations. The maximum required current margin can then be determined, which is used to determine required motor sizing for adequate (Level 1) performance. Step responses are used to evaluate response to piloted commands while gusts are used to evaluate response to a disturbance. The gust inputs take a 1-cosine shape (Ref. 19), with the frequency chosen to maximize motor effort. This frequency is determined by examining the frequency response of input gust to actuator effort (Fig. 6) and choosing the frequency that results in the largest magnitude. This will represent a worst-case gust scenario for motor sizing.

For the inner loop controller, two simulations are considered along the roll/pitch axes in hover: a doublet input in pitch attitude and a gust. The longitudinal and lateral dynamics are identical but for an 18% higher inertia in pitch (Table 2). Thus, only pitch results are presented for the ACAH roll/pitch controller in hover. The doublet input is simulated as a piloted attitude command, and the gust is input directly to the aircraft model.

A truncated step command in the yaw rate is simulated as a piloted input. The gust response is not simulated in the time domain for the yaw axis because gusts in any direction should not cause significant disturbance in the yaw rate due to the symmetry of the aircraft.

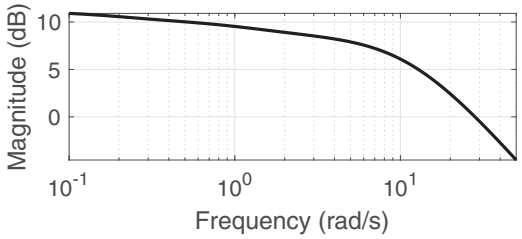

Fig. 7. Magnitude frequency response from vertical gust to motor current.

Similar to the inner loop, for the outer loop (TRC) controller two-time domain simulations are considered along the longitudinal/lateral axes, with only the longitudinal results presented. A small magnitude step in longitudinal flight speed is simulated, as well as a longitudinal gust. The step is simulated as a piloted command while the gust is input to the aircraft model.

The outer loop also controls the heave rate of the aircraft, so a step change in heave rate and a vertical gust are also simulated. Unlike the longitudinal gusts, the magnitude of the frequency response for vertical gust inputs has no clear peak (Fig. 7). The magnitude increases with decreasing vertical gust frequency, meaning that a sustained wind will require the most actuator effort, rather than a short-term gust.

In order to compare aircraft of different sizes, the changes in current and power will be normalized by the hover trim value. The current and power margins are calculated by

$$\left(\frac{\Delta i}{i_{\text{hover}}}\right) = \frac{i - i_{\text{hover}}}{i_{\text{hover}}}, \qquad \left(\frac{\Delta P}{P_{\text{hover}}}\right) = \frac{P - P_{\text{hover}}}{P_{\text{hover}}} \tag{9}$$

In addition to the evaluations from time domain simulations, current margins to meet inner and outer loop OLOP (Ref. 16) requirements are also evaluated. This handling qualities specification determines whether an aircraft is prone to undesired oscillations due to actuator rate saturation. For the multicopters considered in this study, the relevant rate limit is the acceleration of the rotors, which is directly proportional to the maximum current that can be provided to the motors. If a motor is rated for K times the current required to hover, Eq. (3) yields

$$\dot{\Omega}_{\max} = \frac{(K_t i_{\max} - Q_{A,\text{trim}})}{I_{\text{rotor}}} = \frac{(K_t i_{\max} - K_t i_{\text{hover}})}{I_{\text{rotor}}} = \frac{K_t(K-1) i_{\text{hover}}}{I_{\text{rotor}}} \tag{10}$$

By manually reducing K until the OLOP specification is on the Level 1/2 boundary, a minimum required current margin to meet the OLOP specification can be identified using Eq. (11).

$$\left(\frac{\Delta i}{i_{\text{hover}}}\right)_{\text{OLOP}} = (K-1) \tag{11}$$

Results

Inner loop control design

Optimized ACAH controllers are designed for each of the five aircraft cases that meet Level 1 HQ requirements for the specifications listed in Table 3. A full explanation of each of these specifications can be found in Ref. 14.

Tables 6 and 7 give the optimized values of the HQ specifications along the roll, pitch, and yaw axes. Roll and pitch are combined since they are practically identical and use the same gains. The limiting

Table 6. Inner loop HQ (roll/pitch)

Parameter	Unit	1.2 m	1.2 m Scaled	1.8 m	1.8 m Scaled	2.4 m
Stability gain margin	dB	11	13	12	12	13
Stability phase margin	deg	51	57	53	57	49
Bandwidth	rad/s	2.5	3.5	2.5	2.9	2.5
Phase delay	s	0.067	0.044	0.070	0.057	0.084
Crossover frequency	rad/s	5.0	7.1	5.0	5.8	5.0
Disturbance rejection bandwidth	rad/s	1.2	1.3	1.1	1.1	1.2
Disturbance rejection peak	dB	3.5	3.5	3.3	3.5	3.3
Command model following	–	49	42	49	34	49
OLOP phase (pilot)	dB	–	–	–	–	–
OLOP magnitude (pilot)	deg	–	–	–	–	–
OLOP phase (disturbance)	dB	–	−144	–	−153	−137
OLOP magnitude (disturbance)	deg	–	−11.4	–	−15.0	−4.4
Actuator RMS (pilot)	–	0.029	0.082	0.044	0.073	0.049
Actuator RMS (disturbance)	–	0.053	0.111	0.074	0.098	0.113

Note: - indicates no open loop onset point in the frequency range.

Table 7. Inner loop HQ (yaw)

Parameter	Unit	1.2 m	1.2 m Scaled	1.8 m	1.8 m Scaled	2.4 m
Stability gain margin	dB	37	32	35	34	36
Stability phase margin	deg	90	101	102	106	109
Bandwidth	rad/s	1.4	2.0	1.4	1.6	1.4
Phase delay	s	0.002	0.002	0.002	0.002	0.002
Crossover frequency	rad/s	5.0	7.1	5.0	5.8	5.0
Disturbance rejection bandwidth	rad/s	1.0	1.4	1.0	1.1	1.0
Disturbance rejection peak	dB	0.19	0.19	0.23	0.25	0.27
Command model following	–	0.08	0.23	0.07	0.08	0.07
OLOP phase (pilot)	dB	–	–	–	–	–
OLOP magnitude (pilot)	deg	–	–	–	–	–
OLOP phase (disturbance)	dB	−79	−82	−67	−71	−65
OLOP magnitude (disturbance)	deg	−6.01	−1.04	−3.45	−1.02	−2.27
Actuator RMS (pilot)	–	0.080	0.161	0.087	0.114	0.095
Actuator RMS (disturbance)	–	0.49	1.16	0.47	0.67	0.45

Note: - indicates no open loop onset point in the frequency range.

specifications (those near the Level 1/2 boundary) are indicated. Generally, this means that these are the specifications that could be violated if the design parameters were relaxed any further. Regarding the OLOP requirements, some cases have no open loop onset point which is indicated with a dash in the tables.

For all cases, the limiting specification in roll/pitch is the pitch crossover frequency, with the roll bandwidth also on the Level 1/2 boundary. For the aircraft held to the standard specifications, the command model following is limiting for both roll and pitch, but when held to the Froude-scaled requirements, the disturbance rejection bandwidth is limiting instead. Based on the actuator RMS values in roll/pitch, it can be seen that the aircraft held to the scaled specifications require more actuator effort than the unscaled cases of the same size. This is a result of the changes in boundaries for the scaled requirements.

In yaw, the limiting metrics are bandwidth and crossover frequency for all aircraft cases. For piloted inputs, the values of the actuator RMS (a measure of actuator activity, [14]) are lower for the unscaled aircraft. With scaled requirements, actuator activity increases. The yaw actuator RMS is substantially larger than the pitch for all configurations, suggesting a relative lack of authority in this axis.

The current margins required to meet the Level 1 OLOP specifications are given in Table 8. Though there is no onset point for the nominal installed current margin ($\Delta i / i_{\text{hover}} = 1$), the limiting OLOP specification for the inner loop is the pilot yaw input for all cases except the largest aircraft which is limited by the roll disturbance OLOP requirement.

Table 8. Inner loop OLOP current requirements

Rotor Diameter (m)	Current Margin ($\Delta i / i_{\text{hover}}$)	Limiting Input
1.2	0.27	Pilot yaw
1.2 (scaled)	0.57	Pilot yaw
1.8	0.34	Pilot yaw
1.8 (scaled)	0.45	Pilot yaw
2.4	0.51	Roll disturbance

Inner loop time domain simulations (ACAH/RCDH)

Pitch doublet. Figure 8 shows a 10° doublet input (before and after the second-order command filter) in commanded pitch attitude of the quadcopters. The dotted lines indicate the unfiltered step input, while the dashed lines show the filtered command. The magnitude of the doublet does not scale with the size of the quadcopter, but the doublet's duration and the frequency of the command models are Froude scaled. Thus, the smaller quadcopters follow the step more aggressively. For the comparison of the quadcopters without scaling of the HQ requirements, the input given to the largest quadcopter is given to all vehicles.

The closed-loop vehicle responses to the doublet input are plotted in Fig. 9. When all quadcopters are tuned to the same requirements,

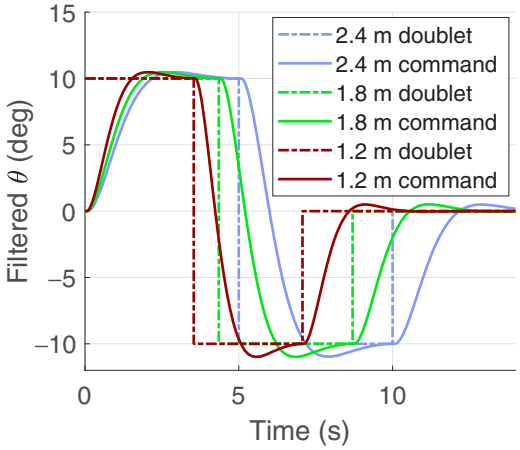

Fig. 8. Filtered pitch attitude doublet input (Froude scaled).

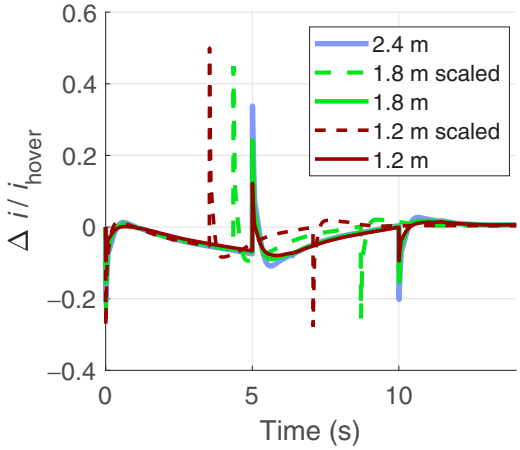

Fig. 10. Motor 3 current for pitch doublet.

they all follow the same trajectory (Fig. 9(a)), settling to their steady-state value in roughly 4 s. When the HQ metrics are Froude-scaled, the smaller quadcopters respond more quickly, though they settle to the same attitude (Fig. 9(b)).

The current required by the rear-left rotor (Motor 3 in Fig. 1) during the pitch doublet is plotted in Fig. 10, normalized by hover current. Each step change in the doublet (at $t = 0$, $t = 5$ s, and $t = 10$ s for the 2.4 m quadcopter) is accompanied by a peak in the current required, as the system tries to rapidly change the rotor thrust through change in rotor speed. Since the largest change in pitch attitude (from $+10^\circ$ to -10°) is commanded in the middle of the doublet, the middle peak in current is also the largest.

When Froude scaling is applied to the HQ requirements for the smallest aircraft, the magnitude of this peak is around 0.5 for a 20° change in the commanded pitch attitude (0.025 per degree), but around 0.3 for the largest aircraft (0.015 per degree). This results from the more aggressive command models on the smaller aircraft. Conversely, when all vehicles are held to the same HQ requirements, the smallest vehicle requires the least current margin. Motor power (not pictured) follows a similar trend. The maximum values of both the normalized current and power are reported for each configuration in Table 9.

Inner loop longitudinal gust. A longitudinal gust is applied to the aircraft in hover to examine how the inner loop controller (ACAH) responds to

Table 9. Maximum current and power input to Motor 3 during pitch doublet

Rotor Diameter (m)	Max $\Delta i/i_{\text{hover}}$	Max $\Delta P/P_{\text{hover}}$
1.2	0.12	0.16
1.2 (scaled)	0.50	0.59
1.8	0.24	0.29
1.8 (scaled)	0.45	0.52
2.4	0.33	0.39

Table 10. Longitudinal Gust Parameters (ACAH)

Rotor Diameter (m)	Frequency (rad/s)	Duration (s)
1.2	6.4	0.98
1.2 (scaled)	10.4	0.60
1.8	6.7	0.94
1.8 (scaled)	8.5	0.74
2.4	6.6	0.95

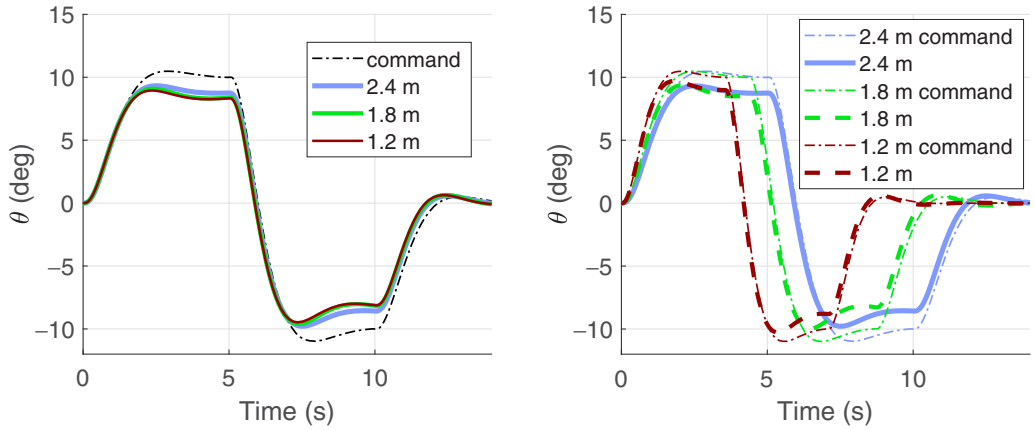

(a) Manned-sized HQ requirements **(b) Scaled HQ requirements**

Fig. 9. Pitch attitude response to doublet input.

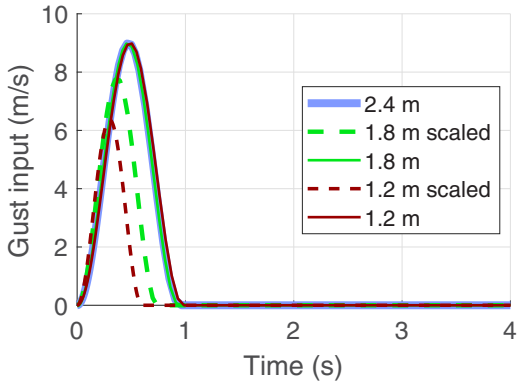

Fig. 11. Longitudinal gust input (attitude hold).

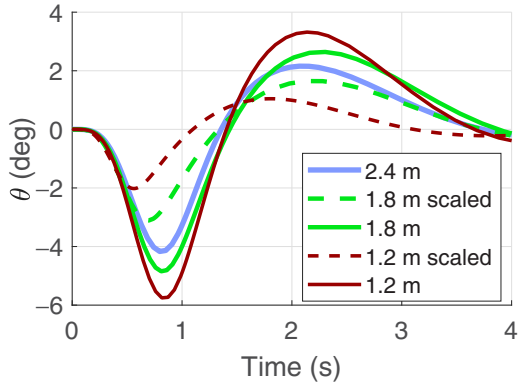

Fig. 12. Pitch attitude response (longitudinal gust).

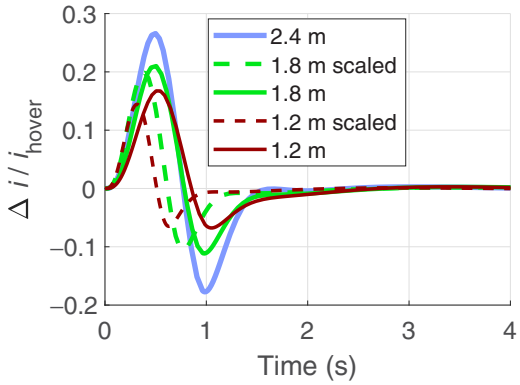

Fig. 13. Motor 1 current for longitudinal gust (ACAH).

a disturbance in aircraft attitude. The gusts for each aircraft case have the parameters in Table 10 and are plotted in Fig. 11. When the HQ metrics are scaled, so too is the magnitude of the gust (larger aircraft are expected to reject larger gusts). All simulated gusts are represented along the aircraft body-reference axis. Thus, a positive longitudinal gust is a tailwind.

The vehicle pitch attitude during the gust is plotted in Fig. 12. The aircraft first pitch nose-down, then nose-up as the ACAH controller brings the attitude back to zero. The current input to the front-right motor (Motor 1 in Fig. 1) during the gust is plotted in Fig. 13. The input to the front motors increases (and the rear decreases) to create a restorative moment that brings the pitch attitude back to zero, with some overshoot as the gust subsides. The magnitude of this input is higher for the larger aircraft as they overcome greater rotor inertia. For the scaled

Table 11. Maximum current and power input to Motor 1 during longitudinal gust (ACAH)

Rotor Diameter (m)	Maximum $\Delta i/i_{\text{hover}}$	Maximum $\Delta P/P_{\text{hover}}$
1.2	0.17	0.29
1.2 (scaled)	0.14	0.24
1.8	0.21	0.33
1.8 (Scaled)	0.20	0.31
2.4	0.27	0.40

cases, the smaller magnitude gust requires less corrective input than the unscaled cases of the same size.

The maximum values of the current and power margins required to reject the gust are given in Table 11. Compared to the current required to execute the 10° doublet maneuver, relatively little current and power input is needed for all aircraft to respond to the longitudinal gust; no vehicle requires more than 27% of the hover current during the longitudinal gust presented (3% per m/s of gust magnitude). This suggests that rejection of such gusts will not be an issue unless significantly larger gust magnitudes are considered.

Yaw rate step. Truncated step commands in yaw rate are simulated for each case. Figures 14 and 15 show the yaw rate and heading response, respectively. All aircraft are able to follow the filtered yaw rate and heading command precisely. The magnitude of the step is determined via Froude scaling (smaller vehicles are expected to achieve higher yaw rates), and the length of the step is set such that the commanded heading change is 100°. Additionally, the time constant of the first-order command filter is lower for the smaller vehicles than for the larger ones (due to higher bandwidth requirements).

The change in current input to the front-right motor during the truncated yaw rate step is shown in Fig. 16 for each aircraft configuration. An initial spike in current is seen around $t = 0$ s as the vehicles increase the torque to the counterclockwise motors (and decrease torque to the clockwise motors) to produce a net moment that rotates the aircraft and achieves the desired yaw rate. A second, negative peak is seen when the step input is truncated. The negative input produces a net torque in the opposite direction, slowing the aircraft until it has stopped rotating.

The peak values of current and power required for the five aircraft cases to track a truncated step in yaw rate are summarized in Table 12. For the aircraft held to the same HQ specifications and given the same step input, the larger aircraft require more current margin due to their higher vehicle inertia.

When held to the scaled HQ specifications and given scaled step inputs, the smaller aircraft require a significantly (twice as much, for the smallest quadcopter) larger change in input current relative to the hover value. This is a result of higher expectations in both yaw rate (smaller aircraft are given larger yaw rate commands) and bandwidth (smaller vehicles are expected to react to commanded yaw rates more quickly). This suggests a lack of yaw authority from the smaller rotors, as the smaller motors struggle to produce enough change in torque to turn the aircraft.

Outer loop control design

As described in Ref. 14, after the ACAH controller is tuned, the inner loop gains (blue box in Fig. 4) are frozen, and an outer loop TRC controller is added to the longitudinal/lateral and vertical axes of the aircraft, as shown by the red box in Fig. 4. The specifications used to optimize the TRC controller are listed in Table 4.

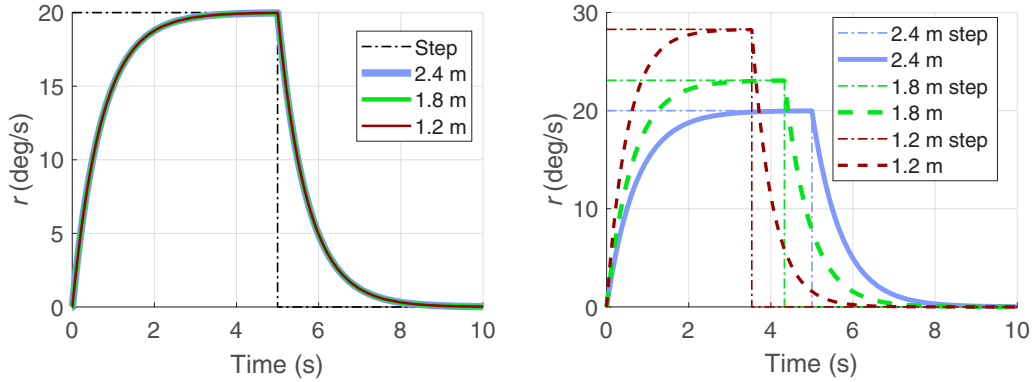

(a) Manned-sized HQ requirements **(b) Scaled HQ requirements**

Fig. 14. Yaw rate response to a truncated step input.

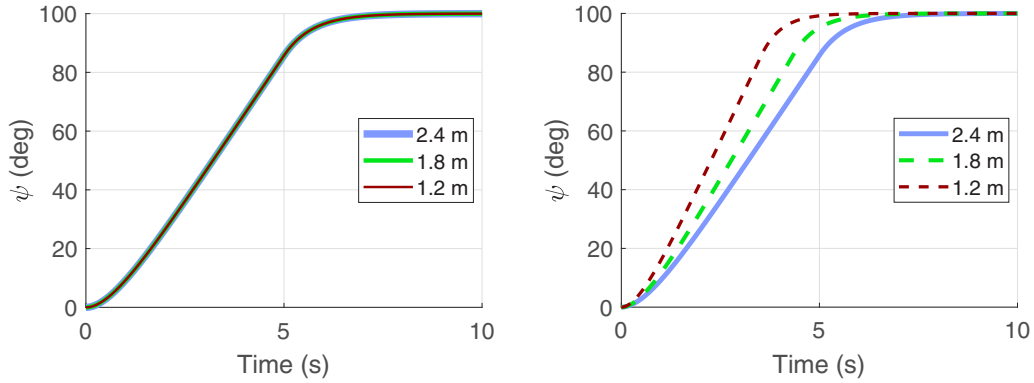

(a) Manned-sized HQ requirements **(b) Scaled HQ requirements**

Fig. 15. Heading response to a truncated step input.

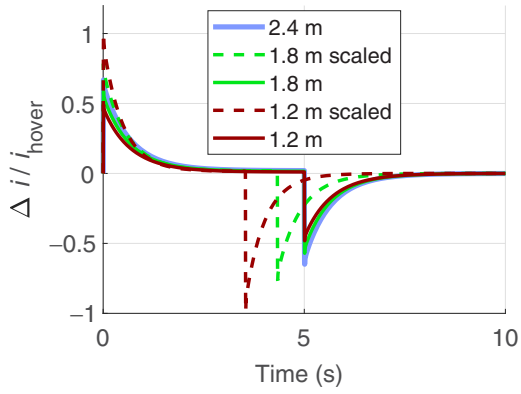

Fig. 16. Motor 1 current for the truncated yaw rate step.

Table 12. Maximum current and power input to Motor 1 during truncated yaw rate step

Rotor Diameter (m)	Maximum $\Delta i/i_{hover}$	Maximum $\Delta P/P_{hover}$
1.2	0.49	0.62
1.2 (scaled)	1.00	1.23
1.8	0.59	0.72
1.8 (scaled)	0.78	0.96
2.4	0.67	0.82

Tables 13 and 14 give the optimized values of the HQ specifications along the longitudinal/lateral and vertical axes, respectively. Since the aircraft are nearly identical along the longitudinal and lateral axes in hover, the same command models and controller gains are used for both axes.

For the longitudinal and lateral axes, the first-order command model is designed such that the value of the rise time falls on the Level 1/2 boundary. The crossover frequency and disturbance rejection peak are the limiting specifications, regardless of whether Froude scaling is applied to the specifications.

In heave, the command model is designed so that the height response characteristics fall on the Level 1/2 boundary. The crossover frequency and disturbance rejection bandwidth are limiting in heave.

As was seen with the inner loop, the outer loop actuator RMS metrics indicate that aircraft held to scaled HQ requirements require more actuator effort than those held to unscaled requirements. This is expected since the scaled cases are required to respond more quickly, as appropriate on a smaller vehicle.

The current margin required to meet the Level 1 OLOP requirements is given in Table 15. For all cases, the heave disturbance onset point is the first to reach the Level 1/2 boundary. Significantly, a less current margin is required to meet the outer loop OLOP requirements than the inner loop OLOP requirements (Table 15).

Outer loop time domain simulations (TRC)

Longitudinal velocity step. The aircraft response to a step command in longitudinal velocity is plotted in Fig. 17 for all cases. The command

Table 13. Outer loop handling qualities (longitudinal/lateral)

Parameter	Unit	1.2 m	1.2 Scaled	1.8 m	1.8 m Scaled	2.4 m
Stability gain margin	dB	8.9	8.5	8.4	8.9	8.4
Stability phase margin	deg	62	56	60	60	55
Crossover frequency	rad/s	1.0	1.4	1.0	1.2	1.0
Disturbance rejection bandwidth	rad/s	0.63	0.85	0.61	0.69	0.60
Disturbance rejection peak	dB	5.0	5.0	5.0	5.0	5.0
Rise time	s	5.0	3.4	5.0	4.2	5.0
Command model following	–	9.1	3.5	9.5	7.1	6.1
OLOP phase (pilot)	deg	–	−327	−332	−309	−284
OLOP magnitude (pilot)	dB	–	−75	−81	−46	−33
OLOP phase (disturbance)	deg	−189	−160	−168	−155	−159
OLOP magnitude (disturbance)	dB	−10	−5.7	−6.7	−5.2	−5.5
Actuator RMS (pilot)	–	0.07	0.11	0.11	0.14	0.15
Actuator RMS (disturbance)	–	0.34	0.57	0.47	0.69	0.62

Note: - indicates no open loop onset point in the frequency range.

Table 14. Outer loop handling qualities (heave)

Parameter	Unit	1.2 m	1.2 m Scaled	1.8 m	1.8 m Scaled	2.4 m
Stability gain margin	dB	51	47	51	49	51
Stability phase margin	deg	88	82	86	84	87
Crossover frequency	rad/s	1.0	1.6	1.0	1.2	1.0
Disturbance rejection bandwidth	rad/s	1.0	1.4	1.0	1.2	1.0
Disturbance rejection peak	dB	0.63	0.83	0.63	0.73	0.63
Heave mode pole	rad/s	0.20	0.29	0.20	0.23	0.20
Time delay	s	0.089	0.085	0.089	0.088	0.089
Command model following	–	0.012	0.006	0.012	0.009	0.012
OLOP phase (pilot)	deg	–	–	–	–	–
OLOP magnitude (pilot)	dB	–	–	–	–	–
OLOP Phase (disturbance)	deg	−107	−106	−102	−102	−99
OLOP Magnitude (disturbance)	dB	−10.2	−6.3	−6.8	−5.0	−4.7
Actuator RMS (pilot)	–	0.05	0.06	0.07	0.08	0.10
Actuator RMS (disturbance)	–	0.47	0.52	0.65	0.70	0.84

Notes: - indicates no open loop onset point in the frequency range.

Table 15. Outer loop OLOP current requirements

Rotor Diameter (m)	Required Current ($\Delta i/i_{\text{hover}}$)	Limiting Input
1.2	0.05	Heave disturbance
1.2 (scaled)	0.10	Heave disturbance
1.8	0.08	Heave disturbance
1.8 (scaled)	0.12	Heave disturbance
2.4	0.10	Heave disturbance

model following for all vehicles is excellent (Table 13), so the filtered commands are omitted. The aircraft that are all held to the manned-sized HQ requirements follow the same step change in flight speed, while the aircraft held to Froude-scaled requirements follow a scaled step. With the application of Froude scaling, the smaller aircraft are not required to go as fast as the larger aircraft, though they are required to settle more quickly as a result of the scaled rise time specification.

In order to achieve the desired flight speed, the quadcopters increase the voltage input to the rear rotors and decrease the input to the front rotors. This pitches the aircraft nose-down, tilting the rotor plane and accelerating the aircraft forward. This pitch response is shown in Fig. 18, with the maximum pitch attitude for all aircraft cases being between -8° and -10° during the step.

The normalized change in current input to the rear-left rotor during the step in longitudinal velocity is plotted in Fig. 19. The input current peaks quickly during the aircraft responses as the controller attempts to pitch the aircraft and accelerate forward. Table 16 gives the maximum values of the required current and power margin (which follows a similar trend as the current).

Even with this relatively small magnitude step, the 1200-lb aircraft and the 680-lb aircraft held to the scaled specifications require a change in current input greater than the nominal hover value ($\Delta i/i_{\text{hover}} > 1$). Though the maximum magnitude of the pitch attitude is similar to the inner loop commands, the frequency of the inner loop command model must be greater in the TRC mode than in the ACAH mode, due to phase margin requirements on the outer loop. Thus, the vehicle responds to the commanded pitch attitude more aggressively, requiring greater current than was seen in the pitch doublet command.

Outer loop longitudinal gust. Similar to what was done with the ACAH controller, a longitudinal gust disturbance is simulated in order to examine the aircraft response. The gust frequencies are chosen based on the magnitude frequency response of the input gust frequency to motor current (similar to Fig. 6). These worst-case gust parameters are given in Table 17. The gust inputs for each aircraft case are shown in Fig. 20. The unscaled cases receive the same gust magnitude and frequency, while the cases held to the scaled HQ requirements receive gusts with Froude-scaled magnitude.

The vehicle pitch attitude during the gust is plotted in Fig. 21, and the longitudinal velocity is plotted in Fig. 22. The gust causes the aircraft to pitch nose-down and begin moving forward. The controllers attempt

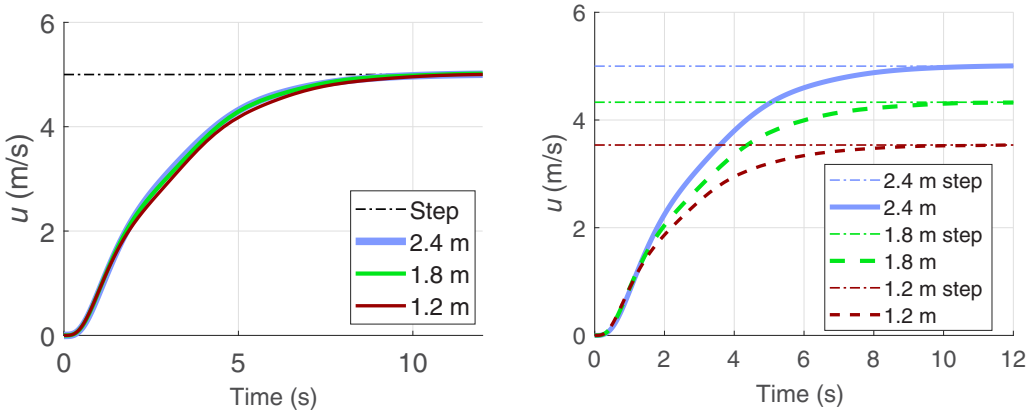

(a) Manned-sized HQ requirements

(b) Scaled HQ requirements

Fig. 17. Longitudinal velocity step response.

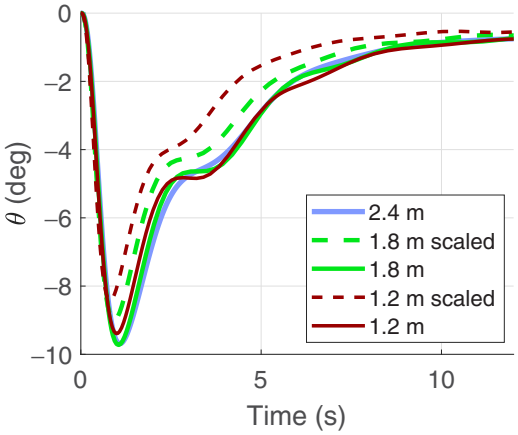

Fig. 18. Pitch attitude during velocity step.

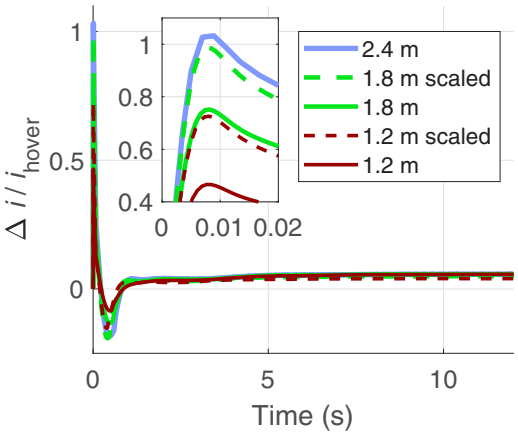

Fig. 19. Motor 3 current for velocity step.

Table 16. Maximum current and power input to Motor 3 during longitudinal step

Rotor Diameter (m)	Maximum $\Delta i/i_{hover}$	Maximum $\Delta P/P_{hover}$
1.2	0.47	0.59
1.2 (scaled)	0.73	0.90
1.8	0.76	0.93
1.8 (scaled)	1.00	1.22
2.4	1.03	1.27

Table 17. Longitudinal gust parameters for peak magnitude current input (TRC)

Rotor Diameter (m)	Frequency (rad/s)	Duration (s)
1.2	6.4	0.98
1.2 (scaled)	8.0	0.79
1.8	6.6	0.95
1.8 (scaled)	7.4	0.85
2.4	6.7	0.94

Table 18. Maximum current and power input to Motor 1 during longitudinal gust (TRC)

Rotor Diameter (m)	Maximum $\Delta i/i_{hover}$	Maximum $\Delta P/P_{hover}$
1.2	0.19	0.32
1.2 (scaled)	0.15	0.26
1.8	0.23	0.36
1.8 (scaled)	0.21	0.33
2.4	0.28	0.42

to return the aircraft to a stationary hover by pitching nose-up to slow the aircraft. With some oscillation, all aircraft cases are brought back to hover in roughly 6 s, with the small vehicles settling faster when their HQ specifications are Froude-scaled.

Figure 23 shows the normalized change in current input to the front-right rotor for each vehicle case during the longitudinal gust with a TRC controller. Similar to the ACAH-mode longitudinal gust, the required changes in current for the aircraft to reject the gust are relatively small. The power input (not pictured) follows a similar trend to the current, and the required values of the current and power margin to reject the longitudinal gust are given in Table 18. The values of the required current and power margin for the TRC controller are approximately the same as those for the attitude-hold controller.

Heave step. A step change in climb rate is simulated on each aircraft case. The step command is filtered to meet the heave response time

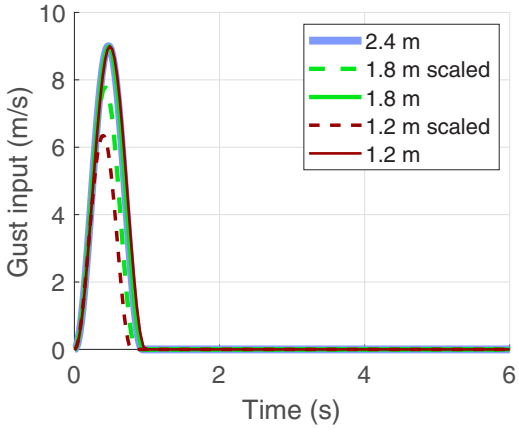

Fig. 20. Longitudinal gust input (TRC).

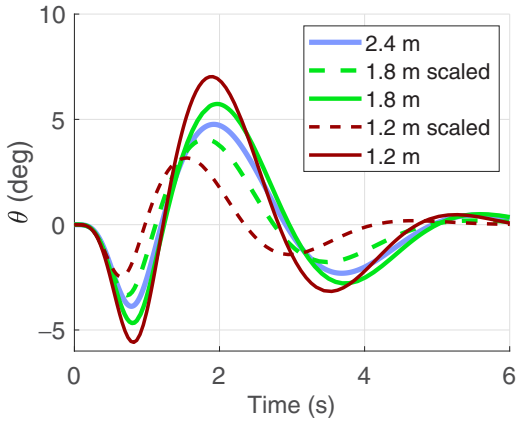

Fig. 21. Pitch response to longitudinal gust (TRC).

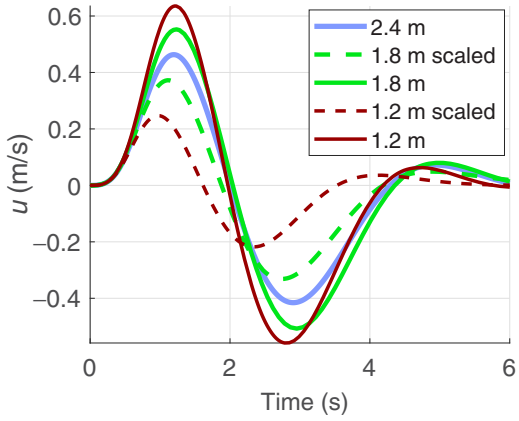

Fig. 22. Response to longitudinal gust (TRC).

constant specification. The aircraft are able to accurately follow the filtered command (Fig. 24). The unscaled cases all have the same response, accurately following the commanded signal and achieving the desired climb rate of 5 m/s (984 ft/min) in about 20 s. For the aircraft held to the Froude-scaled specifications, the smaller aircraft are required to reach a lower velocity in a shorter amount of time.

The normalized changes in current to a single motor during the heave step are shown in Fig. 25. For all cases, the current to all motors spikes at

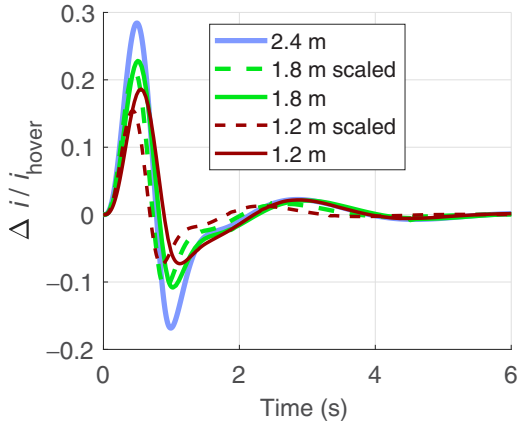

Fig. 23. Motor 1 current for longitudinal gust (TRC).

Table 19. Maximum current and power input to Motor 1 during heave step

Rotor Diameter (m)	Maximum $\Delta i/i_{hover}$	Maximum $\Delta P/P_{hover}$
1.2	0.36	0.46
1.2 (scaled)	0.39	0.49
1.8	0.53	0.66
1.8 (scaled)	0.54	0.67
2.4	0.71	0.86

the beginning of the step as the controller attempts to increase the thrust produced by all rotors to accelerate the aircraft upward and then settles as the aircraft reaches the desired heave rate. The maximum values of both current and power margin required are given in Table 19.

As was the case in the longitudinal axis, the larger aircraft require a larger change in input current, as the larger rotational inertia necessitates greater input to rapidly speed up the larger rotors and produce the required change in thrust. The Froude-scaled cases require only marginally more input than the unscaled cases with the same vehicle size because the more aggressive time constant and time delay required by the Froude-scaled metrics are negated in part by a lower heave rate magnitude. In all cases, the smaller aircraft require less current margin than the larger.

Though the heave step maneuver does not necessarily define the maximum individual rotor current requirement, it is important to consider that in heave this change in current is required for all rotors, whereas in every other axis the current increase to two motors is offset by an equal decrease in the two others. This means that the heave axis will set battery current requirements.

Vertical gust. As described in the Evaluation Methods section, the worst-case vertical gust frequency is a sustained wind, so a step change in gust magnitude is used. The Froude-scaled cases still receive gusts with scaled magnitude, shown in Fig. 26.

Figure 27 shows the aircraft responses to the vertical wind and Fig. 28 shows the normalized change in current input to a single motor. The positive gust magnitude is a downdraft on the aircraft, which causes the rotors to lose thrust. As the aircraft starts to descend (positive w), the controller increases the collective input to increase the speed of all the motors in order to produce more thrust and brings the heave rate back to zero.

All three aircraft sizes held to the same handling qualities specifications have the same heave response and normalized current input when

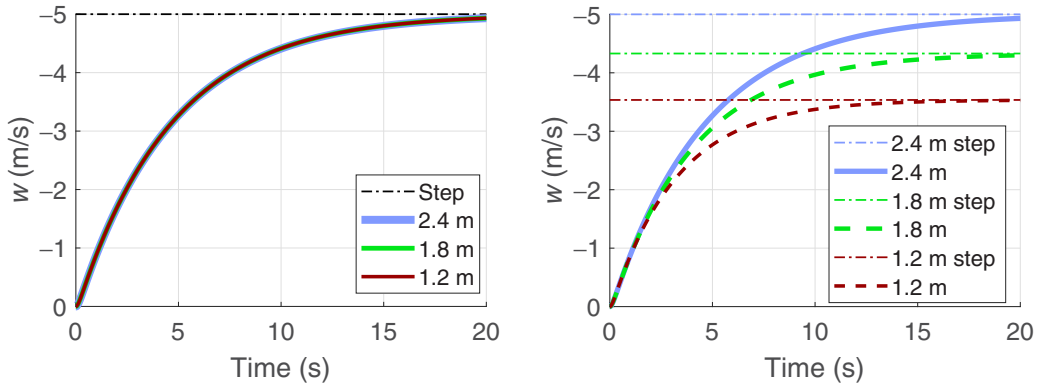

(a) Manned-sized HQ requirements **(b) Scaled HQ requirements**

Fig. 24. Climb rate step response.

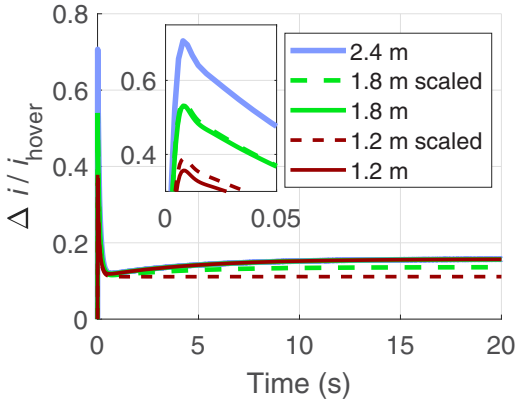

Fig. 25. Current input to Motor 1 during heave step.

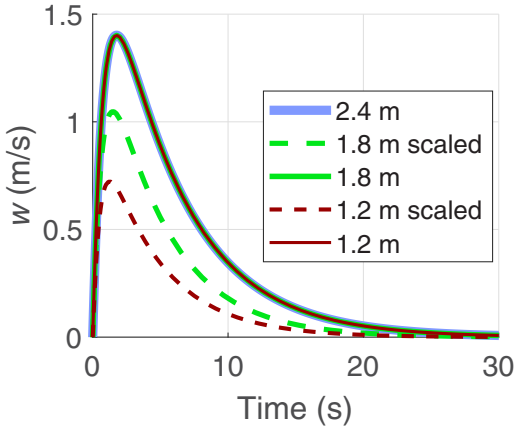

Fig. 27. Response to a vertical gust.

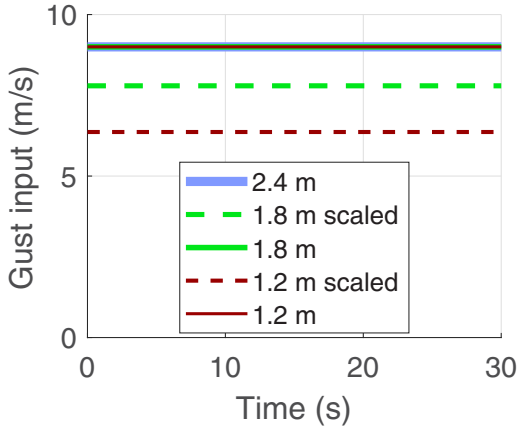

Fig. 26. Vertical gust input.

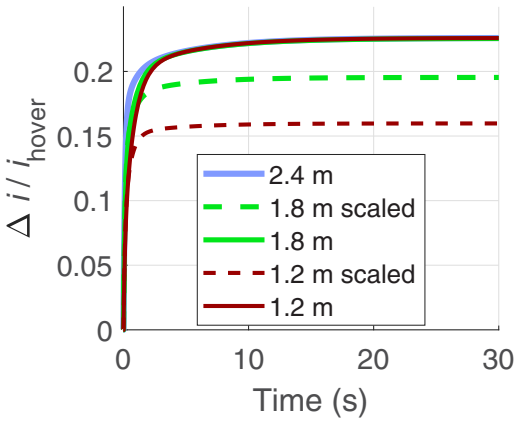

Fig. 28. Motor 1 current during a vertical gust.

given the vertical wind. The aircraft held to the scaled HQ specifications are given a lower magnitude wind and have a lower magnitude response and normalized current input. The required values of current and power margin for each aircraft case to reject the heave gust are given in Table 20.

Limiting cases and motor weight

Required motor weight can be estimated from the maximum current requirement across all time domain simulations for each aircraft case. The required motor torque input is found by multiplying the maximum current (including hover current) by the torque constant. Motor weight can then be estimated using Eq. (12), with Q in N m and M_{motor} in kg (Ref. 20).

$$M_{\text{motor}} = 0.1372 Q^{0.8587} \tag{12}$$

Considering all hover maneuvers, the time simulations that require the largest torque/current are summarized in Table 21, along with

Table 20. Maximum current and power input to Motor 1 during vertical wind

Rotor Diameter (m)	Maximum $\Delta i/i_{hover}$	Maximum $\Delta P/P_{hover}$
1.2	0.23	0.44
1.2 (scaled)	0.16	0.32
1.8	0.23	0.44
1.8 (scaled)	0.20	0.38
2.4	0.23	0.44

the estimated motor masses. Regardless of the scaling of the HQ specification, the smallest aircraft is limited by yaw rate commands, while the step change in longitudinal velocity requires the highest peak current input for the larger two aircraft. This difference is a result of the relative lack of yaw authority of the smaller rotors. The larger aircraft require a higher motor weight fraction than the smaller ones, with the largest quadcopter needing 15.8% of its gross weight to be motors. Naturally, the aircraft held to the Froude-scaled specifications require larger motors than the unscaled cases as a result of the more demanding requirements, though the smaller aircraft still require an overall smaller weight fraction dedicated to motors.

If an ACAH controller is used in the longitudinal/lateral axes instead of the TRC controller for the larger two aircraft (the limiting case for the smallest will not change), the new limiting maneuvers are listed in Table 22. The 680-lb aircraft requires the highest current input during the step in the yaw rate, while the largest aircraft is limited by heave. Without TRC, the largest aircraft now requires a 13.6% motor weight fraction and the smaller aircraft require less. As the smallest vehicle was not limited by the TRC controller, its required motor weight does not change.

It is worth noting that the weight fractions quoted in Tables 21 and 22 include only the four motors. Additional support structure and cabling will increase the overall powertrain weight even further.

Sensitivity to rotor inertia

Rotor inertia is estimated from data from existing multicopter rotors, but little data are available for rotors suited for UAM applications (over 1 m diameter). Thus, the sensitivity of the motor sizing to changes in rotor inertia is examined.

For the single passenger scale aircraft, the time simulations seen previously to be limiting motor requirements (longitudinal/lateral velocity step, heave rate step, and yaw rate step) are rerun with rotor inertias of 50%, 75%, 125%, and 150% of the nominal rotor inertia. Changes in rotor inertia only directly affect the stability/control derivatives related to the rotor speed, and these dynamics are inverted by the feed-forward RPM controller, so the inner/outer loop dynamics are unaffected. So, though changes in rotor inertia do not change aircraft response to the inputs, they do result in changes in input current.

Table 23. Maximum current for 1200 lb aircraft with varied rotor inertia (longitudinal/lateral velocity step)

Change from Baseline Inertia	Maximum $\Delta i/i_{hover}$	Change from Baseline	Maximum Current (A)	Maximum Torque (N-m)
−50%	0.52	−49.5%	228	269
−25%	0.78	−24.3%	267	315
Baseline	1.03	–	305	360
+25%	1.29	+25.2%	344	406
+50%	1.55	+50.5%	383	452

Table 24. Maximum current for 1200 lb aircraft with varied rotor inertia (heave rate step)

Change from Baseline Inertia	Maximum $\Delta i/i_{hover}$	Change from Baseline	Maximum Current (A)	Maximum Torque (N-m)
−50%	0.35	−50.7%	203	240
−25%	0.53	−25.4%	230	272
Baseline	0.71	–	257	303
+25%	0.88	+23.9%	282	333
+50%	1.04	+47.5%	306	361

Table 25. Maximum current for 1200 lb aircraft with varied rotor inertia (yaw rate step)

Change from Baseline Inertia	Maximum $\Delta i/i_{hover}$	Change from Baseline	Maximum Current (A)	Maximum Torque (N-m)
−50%	0.642	−3.5%	246	291
−25%	0.657	−1.2%	249	294
Baseline	0.665	–	250	295
+25%	0.671	+0.9%	251	296
+50%	0.674	+1.4%	251	297

Table 21. Maximum current and motor mass with TRC

Rotor Diameter (m)	Maneuver	Maximum Current (A)	Maximum Torque (N-m)	Motor Mass (kg)	Weight Fraction (%)
1.2	Yaw rate step	112	34	2.8	8.3
1.2 (scaled)	Yaw rate step	150	45	3.6	10.6
1.8	Longitudinal velocity step	197	130	9.0	11.6
1.8 (scaled)	Longitudinal velocity step	224	148	10.0	13.0
2.4	Longitudinal velocity step	305	360	21.5	15.8

Table 22. Maximum current and motor mass without TRC

Rotor Diameter (m)	Maneuver	Maximum Current (A)	Maximum Torque (N-m)	Motor Mass (kg)	Weight Fraction (%)
1.8	Yaw rate step	178	118	8.3	10.7
1.8 (scaled)	Yaw rate step	199	132	9.1	11.8
2.4	Heave rate step	257	303	18.5	13.6

Table 26. Motor mass of 1200 lb aircraft with varied rotor inertia (TRC)

Change from Baseline Inertia	Maneuver	Motor Mass (kg)	Weight Fraction	Change from Baseline
−50%	Yaw rate step	17.9	13.2%	−2.6%
−25%	Longitudinal/lateral velocity step	19.2	14.1%	−1.7%
Baseline	Longitudinal/lateral velocity step	21.5	15.8%	–
+25%	Longitudinal/lateral velocity step	23.8	17.5%	+1.7%
+50%	Longitudinal/lateral velocity step	26.1	19.2%	+3.4%

Table 27. Motor Mass of 1200 lb Aircraft with Varied Rotor Inertia (without TRC)

Change from Baseline Inertia	Maneuver	Motor Mass (kg)	Weight Fraction	Change from Baseline
−50%	Yaw rate step	17.9	13.2%	−0.5%
−25%	Yaw rate step	18.1	13.3%	−0.3%
Baseline	Heave rate step	18.5	13.6%	–
+25%	Heave rate step	20.1	14.8%	+1.2%
+50%	Heave rate step	21.6	15.9%	+2.2%

The resulting current margins (and motor torques) are given in Tables 23–25 for the three limiting time domain simulations. For the longitudinal velocity step and heave rate step (maneuvers that rely on a change in rotor RPM), the percent change in required current margin and motor torque is roughly equal to the percent change in rotor inertia. However, regarding the yaw axis, changing the rotor inertia only marginally changes the required current margin. This is due to changes in yaw rate being dependent on changes in differential motor torque, rather than changes in rotor speed.

The limiting specifications and subsequent motor weight requirements for the 1200-lb aircraft with varied rotor inertia are given in Table 26. Significantly reducing the rotor inertia (50% of baseline) causes the yaw rate step to become the limiting maneuver. This is due to the current margin required by the yaw rate step being significantly less sensitive to changes in rotor inertia than the longitudinal/lateral velocity step. Reducing the rotor inertia can reduce the required motor weight by up to about 17% for a 50% reduction in rotor inertia, though further reduction of rotor inertia would not cause a significant change in the required weight fraction, as the yaw rate step becomes limiting.

Changing the longitudinal controller to be ACAH rather than TRC reduces the required current margin and subsequent motor weight, as step changes in velocity are no longer directly commanded. The new limiting maneuvers as well as motor weight fraction without the TRC controller are given in Table 27. For the baseline case, and increased rotor inertia, the heave rate step becomes limiting, but at lower rotor inertia the yaw rate step is limiting. In this flight mode, reducing the rotor inertia results in only small changes in motor weight fraction, due to the yaw rate step being limiting.

Effects of additional filtering

For the longitudinal velocity and heave rate step simulations, the maximum current occurs as a spike within the first tenth of a second. The rotor speeds are commanded to increase very quickly at the beginning of these simulations in order to accelerate the aircraft, causing the spikes in input current. This spike can be alleviated by increasing the order of the RPM command model (Ω command model in Fig. 4). Making this command model second order will allow the rotor speeds to accelerate more slowly at the beginning of the step responses, reducing the magnitude of the current spike.

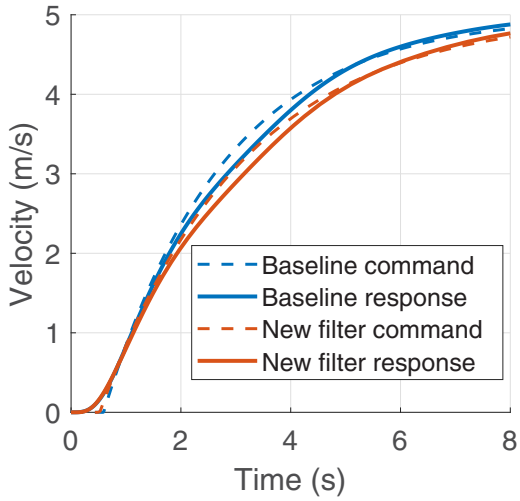

Fig. 29. Longitudinal velocity response.

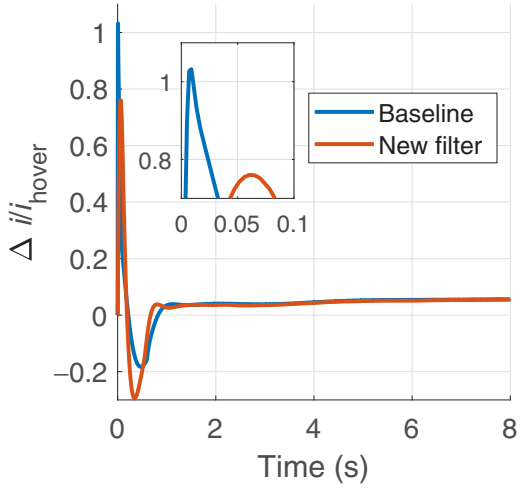

Fig. 30. Current for longitudinal velocity step.

The controller of the 1200-lb quadcopter is redesigned using CONDUIT® with a second-order RPM command model. A damping ratio of 0.707 is used, with the frequency optimized as a design parameter. The aircraft response to the longitudinal velocity step with the baseline and new, second-order RPM command model is shown in Fig. 29 with the current shown in Fig. 30. With the new RPM command model, the peak current drawn by the motor is reduced by 26%.

The increase in the order of the RPM command model also reduces the initial peak in current during the heave rate step response. The aircraft response to the heave rate step with the baseline and new RPM command model is shown in Fig. 31 with the current shown in Fig. 32. With the new

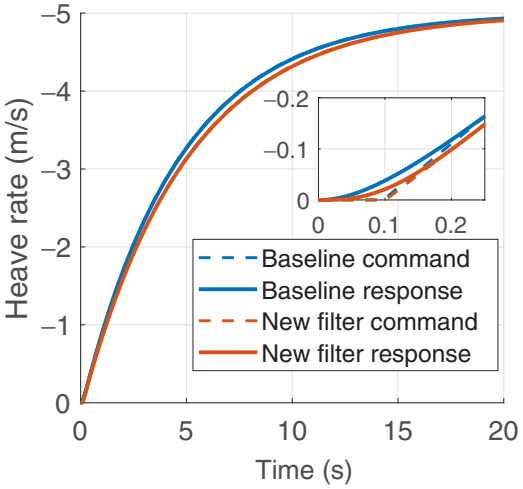

Fig. 31. Heave rate response.

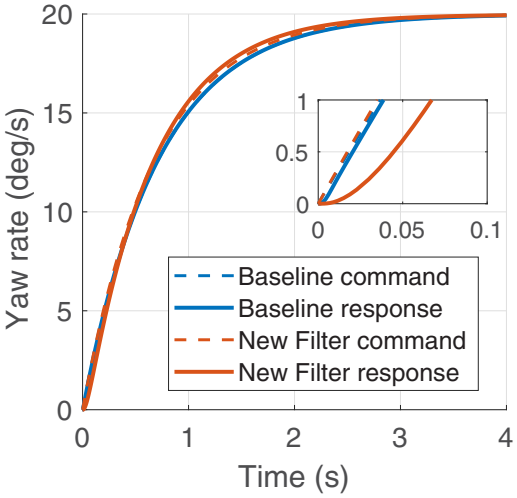

Fig. 33. Yaw rate step response.

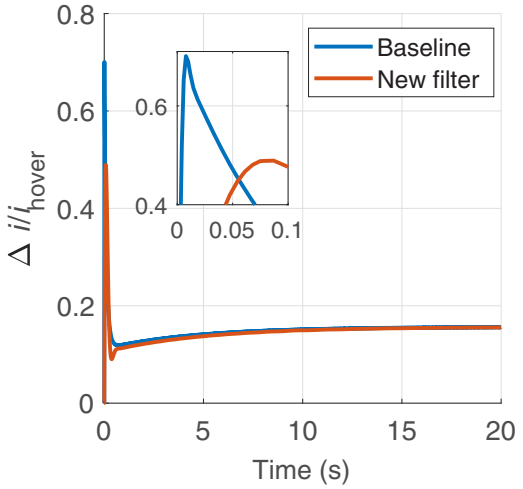

Fig. 32. Current for heave rate step.

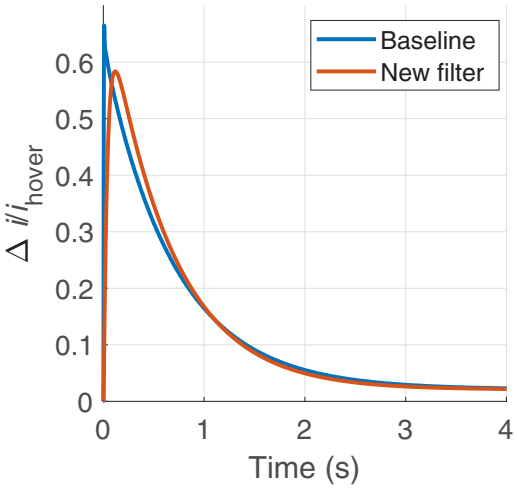

Fig. 34. Current for the yaw rate step.

RPM command model, the peak current drawn by the motor is reduced by 30%. Unlike the longitudinal velocity and heave rate step, the second-order RPM command filter will not affect the peak in current seen in the yaw rate step response. This is due to the differential command being fed directly into the actuator model, bypassing the RPM command model. This is done because the yaw response relies directly on changes in torque, rather than changes in rotor speed.

Rather than changing the RPM command model, the peak in current that occurs during the yaw rate step can be alleviated by adding a low pass filter on the feed-forward path. This reduces the commanded yaw acceleration at the beginning of the command, lowering the required current input. The controller of the 1200 lb is again redesigned using CONDUIT®, with the frequency of a low pass filter in the yaw feed-forward path as an additional design parameter. The aircraft response to a yaw rate step command with the addition of the low pass filter is shown in Fig. 33 with the current shown in Fig. 34. With the low pass filter, the peak current drawn by the motor is reduced by 12%.

The changes in required current margin for the limiting maneuvers with the second-order RPM command model and yaw feed-forward low pass filter are summarized in Table 28. The resulting required motor mass with additional filtering is given in Table 29. With TRC control, the required motor weight of the 1200-lb aircraft is reduced by about 12% with the additional filtering. Without TRC control, the motor weight is reduced by 6.5% with the yaw rate step becoming the limiting maneuver.

Summary and Discussion

Optimized inner and outer loop controllers were designed holding three quadcopters of different sizes to standard and Froude-scaled ADS-33E-PRF HQ specifications. For the inner loop, all aircraft cases are able to meet the Level 1 HQ specifications along the roll/pitch axes with ACAH/RCDH control. When Froude scaling is applied, smaller aircraft require less current margin to reject a longitudinal gust than the larger aircraft, but the opposite is true for a doublet input in pitch attitude.

All cases are also able to meet the Level 1 HQ specifications with an RCDH controller in yaw. When Froude scaling is applied, the smaller aircraft require a significantly higher current margin to follow a truncated step in yaw rate, suggesting a relative lack of yaw authority with the smaller rotors.

For the outer loop, all aircraft cases are able to meet the Level 1 HQ specifications with a TRC controller on the longitudinal/lateral axes. It was seen that:

Table 28. Maximum current for 1200 lb aircraft with additional filtering

	Maneuver	Max $\Delta i/i_{hover}$	Maximum Current (A)	Maximum Torque (N-m)
Baseline	Longitudinal/lateral	1.03	305	360
second-order RPM command	Velocity step	0.76	264	312
Baseline	Heave rate	0.71	257	303
second-order RPM command	Step	0.49	224	264
Baseline	Yaw rate	0.67	250	295
yaw low-pass filter	Step	0.58	237	280

Table 29. Motor MASS of 1200 lb aircraft with additional filtering

Case	Maneuver	Motor Mass (kg)	Weight Fraction	Change from Baseline
Baseline (TRC)	Longitudinal/lateral velocity step	21.5	15.8%	–
Additional filtering (TRC)	Longitudinal/lateral velocity step	19.0	14.0%	−1.8%
Baseline (without TRC)	Heave rate step	18.5	13.6%	–
Additional filtering (without TRC)	Yaw rate step	17.3	12.7%	−0.9%

1) The larger aircraft require a large current margin during a step command in longitudinal velocity as a result of the large rotational acceleration required, with the value of current margin exceeding 1 for the 2.4-m diameter rotors and Froude-scaled 1.8 m diameter rotors.

2) Though higher than that of the ACAH control, rejection of a longitudinal/lateral gust with a TRC controller requires less current margin than following a step command in velocity.

All aircraft cases are also able to meet the Level 1 HQ specifications with a rate-command controller in heave. It was seen that

1) The larger aircraft require a higher current margin during a step-in heave rate than the smaller vehicles.

2) The heave axis will be limiting for battery current requirements.

3) The worst-case gust frequency in heave is a sustained wind, but even this requires a relatively low current margin for all cases.

The values of maximum current input from the time simulations were used to estimate the motor size. With TRC control, it was seen that the longitudinal velocity step was the maneuver that required the highest individual current input for the larger two aircraft cases as a result of the large pitch rotational acceleration required during the step, while the 300-lb aircraft was limited by the yaw rate step. It is concluded that control (with satisfactory HQ) of fixed-pitch, variable-RPM quadcopters capable of manned operations is feasible, but requires relatively higher motor weight as compared to smaller, unmanned vehicles. Using the maximum current values from simulation, the smallest aircraft with 4 ft diameter rotors required 8.3% motor weight fraction (10.6% with scaled specifications), the aircraft with 6 ft diameter rotors requires 11.6% motor weight fraction (13.0% with scaled specifications) and the aircraft with 8 ft diameter rotors requires a motor weight fraction of 15.8%. Motor weight requirements can be somewhat reduced for the larger two aircraft by flying exclusively in ACAH mode instead of TRC mode. In this case, step commands in yaw rate are limiting for the 1.8-m aircraft (requiring 10.7% to 11.8% weight fraction) and heave commands are limiting for the largest vehicles, requiring 13.6% motor weight fraction.

Some design strategies for reducing the required motor weight fraction were considered on the 1200-lb aircraft and it was found that

1) The required current margin for longitudinal/lateral velocity and heave rate step responses tends to change proportionally with rotor inertia.

2) Changing rotor inertia had marginal effects on the current required for yaw commands.

3) Changing the RPM command model to be second-order reduces rotor rotational acceleration requirements for the longitudinal/lateral velocity and heave rate step responses, lowering the initial peak in current.

4) Introducing a low pass filter in the feed-forward path of the yaw controller reduces the initial peak in current by allowing for a slower acceleration in the yaw.

Conclusions

Optimized inner and outer loop controllers were designed using CONDUIT® that met Level 1 specifications for quadcopters in hover with rotor diameters of 1.2, 1.8, and 2.4 m (gross weights of 136, 308, and 544 kg). All aircraft were first held to standard, manned-sized ADS-33E-PRF HQ specifications. Then, Froude scaling was applied to scale the HQ requirements of the two smaller aircraft to that of the manned-sized aircraft. Piloted step commands and gust disturbances were simulated in the time domain (for both Froude-scaled and unscaled cases) in order to determine the maximum motor current margin required for appropriate maneuverability in hover and low speed. It was concluded that

1) For quadcopters smaller than the manned-sized scale, Froude scaling can be used to represent a more aggressive scenario for motor sizing.

2) Yaw requirements are limiting for smaller vehicles due to the smaller motors producing less differential torque, as compared to rotor thrust in the other axes.

3) For the manned-sized quadcopter, longitudinal/lateral and heave acceleration requirements are the limiting maneuver for motor sizing.

4) Control of fixed-pitch, variable-RPM quadcopters capable of manned operations is feasible but requires higher motor weight compared to smaller vehicles (15.8% vs. 13.6% motor weight fraction).

5) Motor weight for UAM-scale quadcopters can be reduced if flown with ACAH longitudinal/lateral controller instead of TRC.

6) Required current margin may be reduced by lowering rotor inertia, up until the point where yaw response becomes limiting.

7) Additional filtering of commands can reduce the peaks in current input by lowering the required rotor acceleration.

Acknowledgments

This work is carried out at Rensselaer Polytechnic Institute under the Army/Navy/NASA Vertical Lift Research Center of Excellence

(VLRCOE) Program, grant number W911W61120012, with Dr. Mahendra Bhagwat as Technical Monitor. The authors would like to acknowledge the Army Combat Capabilities Development Command for sponsoring Ms. Ariel Walter through the Science Mathematics And Research Transformation (SMART) Scholarship Program as well as the Army Research Office for sponsoring Mr. Michael McKay through the National Defense Science and Engineering Graduate Fellowship (NDSEG).

References

[1]Johnson, W., Silva, C., and Solis, E., "Concept Vehicles for VTOL Air Taxi Operations," Proceedings of the AHS Technical Conference on Aeromechanics Design for Transformative Flight, San Francisco, CA, January 16–18, 2018.

[2]"Aeronautical Design Standard, Performance Specification, Handling Qualities Requirements for Military Rotorcraft," ADS-33E-PRF, 2000.

[3]Walter, A., McKay, M., Niemiec, R., Gandhi, F., and Ivler, C., "Handling Qualities Based Assessment of Scalability for Variable-RPM Electric Multi-Rotor Aircraft," Proceedings of the 75th Annual Forum of the Vertical Flight Society, Philadelphia, PA, May 13–16, 2019.

[4]Malpica, C., and Withrow-Maser, S., "Handling Qualities Analysis of Blade Pitch and Rotor Speed Controlled eVTOL Quadrotor Concepts for Urban Air Mobility," Proceedings of the Vertical Flight Society International Powered Lift Conference, San Jose, CA, January 21–23, 2020.

[5]Niemiec, R., Gandhi, F., Lopez, M., and Tischler, M., "System Identification and Handling Qualities Predictions of an eVTOL Urban Air Mobility Aircraft Using Modern Flight Control Methods," Proceedings of the 76th Annual Forum of the Vertical Flight Society, Virtual, October 6–8, 2020.

[6]Ivler, C., Goerzen, C., Wagster, J., Sanders, F., Cheung, K., and Tischler, M., "Control Design for Tracking of Scaled MTE Trajectories on an IRIS+ Quadrotor," Proceedings of the 74th Annual Forum of the American Helicopter Society, Mesa, AZ, May 14–17, 2018.

[7]McKay, M., Niemiec, R., and Gandhi, F., "Performance Comparison of Quadctopers with Variable-RPM and Variable-Pitch Rotors," *Journal of the American Helicopter Society*, Vol. 64, (4), 2019, pp. 1–14. DOI: 4050/JAHS 64.042006.

[8]Walter, A., McKay, M., Niemiec, R., Gandhi, F., Hamilton, C., and Jaran, C., "An Assessment of Heave Response Dynamics for Electrically Driven Rotors of Increasing Diameter," Proceedings of the Autonomous VTOL Technical Meeting & eVTOL Symposium, Mesa, AZ, January 9–11, 2019.

[9]Reddinger, J.-P., "Coupled Pitch-Lag Hinge for High Inertia Electric Rotors," Proceedings of the 76th Annual Forum of the Vertical Flight Society, Virtual, October 6–8, 2020.

[10]Niemiec, R., and Gandhi, F., "Development and Validation of the Rensselaer Multicopter Analysis Code (RMAC): A Physics-Based Comprehensive Modeling Tool," Proceedings of the 75th Annual Forum of the Vertical Flight Society, Philadelphia, PA, May 13–16, 2019.

[11]Peters, D., Boyd, D., and He, C., "Finite-State Induced-Flow Model for Rotors in Hover and Forward Flight," *Journal of the American Helicopter Society*, Vol. 34, (4), 1989, pp. 5–17. DOI: 10.4050/JAHS.34.5.

[12]Niemiec, R., "Development and Application of a Medium-Fidelity Analysis Code for Multicopter Aerodynamics and Flight Mechanics," Ph.D. Thesis, Rensselaer Polytechnic Institute, 2018.

[13]Niemiec, R., and Gandhi, F., "Multi-Rotor Coordinate Transform for Orthogonal Primary and Redundant Control Modes for Regular Hexacopters and Octocopters," Proceedings of the 42nd European Rotorcraft Forum, Lille, France, September 5–8, 2016.

[14]Tischler, M., Berger, T., Ivler, C., Mansur, M., Cheung, K., and Soong, J., *Practical Methods for Aircraft and Rotorcraft Flight Control Design: An Optimization-Based Approach*, AIAA Education Series, AIAA, Reston, VA, 2017.

[15]Berger, T., Ivler, C., Berrios, M., Tischler, M., and Miller, D., "Disturbance Rejection Handling-Qualities Criteria for Rotorcraft," Proceedings of the 72nd Annual Forum of the American Helicopter Society, West Palm Beach, FL, May 16–19, 2016.

[16]Duda, H., "Flight Control System Design Considering Rate Saturation," *Aerospace Science and Technology*, Vol. 2, (4), 1998, pp. 265–275. DOI: 10.1016/S1270-9638(98)80004-7.

[17]Tischler, M., and Remple, R., *Aircraft and Rotorcraft System Identification*, AIAA Education Series, AIAA, Reston, VA, 2012.

[18]Alvarenga, J., Vitzilaios, N., Rutherford, M., and Valavanis, K., "Scaled Control Performance Benchmarks and Maneuvers for Small-Scale Unmanned Helicopters," Proceedings of the IEEE 54th Annual Conference on Decision and Control, Osaka, Japan, December 15–18, 2015.

[19]Berrios, M., Berger, T., Tischler, M., Juhasz, O., and Sanders, F., "Hover Flight Control Design for UAS Using Performance-based Disturbance Rejection Requirements," Proceedings of the 73rd Annual Forum of the American Helicopter Society, Fort Worth, TX, May 9–11, 2017.

[20]Johnson, W., "NDARC – NASA Design and Analysis of Rotorcraft," NASA TP 218751, 2015.